Journal Pre-proof

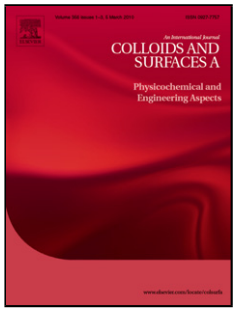

Montmorillonite- hydrothermal carbon nanocomposites: synthesis, characterization and evaluation of pesticides retention for potential treatment of agricultural wastewater

M.E. Zelaya Soulé, M.A. Fernández, M.L. Montes, F. Suárez-García, R.M. Torres Sánchez, J.M. D. Tascón

PII: S0927-7757(19)31185-9

DOI: https://doi.org/10.1016/j.colsurfa.2019.124192

Reference: COLSUA 124192

To appear in: *Colloids and Surfaces A: Physicochemical and Engineering Aspects*

Received Date: 5 August 2019

Revised Date: 31 October 2019

Accepted Date: 3 November 2019

Please cite this article as: Soulé Z, Fernández MA, Montes ML, Suárez-García F, Torres Sánchez RM, Tascón JMD, Montmorillonite- hydrothermal carbon nanocomposites: synthesis, characterization and evaluation of pesticides retention for potential treatment of agricultural wastewater, *Colloids and Surfaces A: Physicochemical and Engineering Aspects* (2019), doi: https://doi.org/10.1016/j.colsurfa.2019.124192

Montmorillonite- hydrothermal carbon nanocomposites: synthesis, characterization and evaluation of pesticides retention for potential treatment of agricultural wastewater

M.E. Zelaya Soulé[a], M.A. Fernández[a], M.L. Montes[b], F. Suárez-García[c], R.M. Torres Sánchez[a] and J.M. D. Tascón[c]

[a]*Centro de Tecnología de Recursos Minerales y Cerámica. CETMIC, CIC-CONICET CCT-La Plata, Camino Centenario y 506- M.B. Gonnet, Argentina.*
[b]*IFLP, CONICET CCT-La Plata, UNLP, La Plata, Argentina.*
[c]*Instituto Nacional del Carbón, INCAR-CSIC, Francisco Pintado Fe, 26, 33011, Oviedo, España.*

emizelayasoule@gmail.com, marielafernandez0712@gmail.com, mlucianamontes@gmail.com, fabian@incar.csic.es, rosa.torres@gmail.com, tascon@incar.csic.es

Graphical abstract

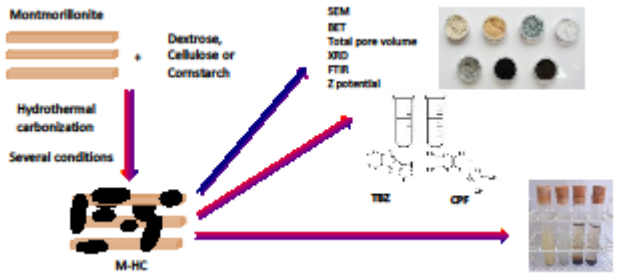

Abstract

Montmorillonite (M) was modified by addition of hydrothermal carbon (HC) in order to obtain pesticide adsorbent materials. Carbohydrates were used as carbon source, and in some cases, also phosphoric acid was applied as activation agent. The M-HC hybrids maintain the negative electrical surface charge of their precursors (between -35 mV and -15 mV), while lower specific surface areas (around 6 m^2 g^{-1}) than that of M sample (66 m^2 g^{-1}) were found. The loss of specific surface could be assigned to the carbon location on both the external and the interlayer surface of the M sheets, as was confirmed by FTIR, zeta potential measurements and XRD analysis. For M-HC products obtained by acid treatment, despite their structure alteration, the specific surface values remained similar to that of M sample (around 70 m^2 g^{-1}).

The M-HC products with or without acid treatment retain almost 100 % adsorption of chlorpyrifos (CPF) and thiabendazole (TBZ) as that obtained for M sample, under the tested conditions. Coagulation studies revealed that M-HC products evaluated showed better precipitation property than that of M sample, which would preclude the typical montmorillonite gel formation that usually block filters and reactors.

Keywords: hydrothermal carbon, montmorillonite, thiabendazole, chlorpyrifos

1. Introduction

Human activity generates wastewaters that cause environmental pollution. In particular, farming activities use pesticides for crops, achieving groundwater or surface water-bodies by runoff, infiltration and/or containers washing (Regaldo et al., 2018). The water contamination with pesticides and possible damage of living beings' health has raised scientific concern, revealing the need of remediation of the polluted water through water

purification systems. In this sense, the optimization and development of advanced technologies are crucial to meet the current and future water needs (Geise et al., 2010)

The low cost and easy access of clay minerals allow their use as adsorbents of a wide variety of pollutants. Among them, montmorillonite clay (M) stands out because in addition to its laminar structure, presents large surface area and cation exchange capacity (Lagaly et al., 2006). Nevertheless, its use as filter is controversial due to its swelling property, which produces an increase in filter resistance by gel formation (Basnayaka et al., 2018). Besides in batch conditions, the M relatively low coagulation property difficult its recuperation from the treatment reactors (Santiago et al., 2016). The surface modification of M sample by some carbon coating would change some of its properties, as swelling capacity decrease (as reported for a Nigerian bentonite modified by dodecyltrimethylammonium bromide (Chikwe et al., 2018)) or coagulation increase, allowing its use in filters and reactors, without losing or even increasing the adsorption capacity of both.

Several methods were employed for the treatment of wastewater intended for agricultural use, based on adsorption processes, such as filters and batch processes (Capra and Scicolone, 2004; Gottschall et al., 2007; Jiménez et al., 1999). While for the treatment of agricultural wastewater, the use of M and organo-montmorillonites as adsorbents has proven successful (Gamba et al., 2017, 2015; Gu et al., 2015; Nir et al., 2000).

Activated carbon materials have a well-developed internal pore structure and various functional groups on their surface, which allowed them to be widely used as adsorbents, catalysts and catalyst carriers (Liu et al., 2010). A cheaper alternative and environmentally friendly method to attain carbon has been developed recently by hydrothermal carbonization (HTC) treatment of biomass saturated with water, at mild reaction conditions (≤ 350 °C and ≤ 20 MPa) (Guo et al., 2016; Titirici and Antonietti, 2010). During the treatment, oxygen functional groups decomposed, leading to dehydration and increasing the heating value (Zheng et al., 2017). The hydrothermal treatment of carbohydrates produces their aromatization, generating products in the form of micrometric spheres with a large number of OH^- and CO^- groups (Liu et al., 2010). Hydrothermal carbonizaton has been carried out in the presence of e.g. graphene oxide (GO) nanosheets (Martín-Jimeno et al., 2015), more recently in the presence of montmorillonite (Li et al., 2014), zeolites (Gao et al., 2005) and silica gel (Gun'ko et al., 2004). In the first case, GO acted as a morphology-directing agent and a hybrid HC-GO material formed by a thin layer of hydrothermal carbon was obtained on the CO sheets. In the second case, a composite material of hydrothermal carbon nanospheres supported on montmorillonite was prepared. Besides, several works conclude that parameters as temperature, time and acid type and concentration are relevant in the achieved characteristic of the synthetized materials (Chham et al., 2018; Kausar et al., 2018; Mansouri et al., 2018; Toor and Jin, 2012).

Several chemical agents are used to safeguard agricultural commodities against fungi, insects and herbs (Abbas et al., 2018), although various studies highlighted their genotoxic and mutagenic effects (Abbas et al., 2018; Iqbal, 2016). In particular, the wide use in Argentina of the insecticide chlorpyrifos (CPF) for crop protection (Hunt et al., 2016; Marino and Ronco, 2005), and the fungicide thiabendazole (TBZ) for fruit protection (Lombardi et al., 2003), generates an important environmental concern. Particularly, to obtain a good dispersion of this insecticide, it is sprayed as fine particles suspended in an aqueous medium. Its application by spraying in the atmosphere generates by means of rain or irrigation its leachate below the root zone, reaching and contaminating groundwater and / or surface water (Haynes et al., 2000; Schipper et al., 2008), making its removal very difficult. While residues from the washes of insecticides containers, and the application of fungicides in fruit packing plants (Gamba et al., 2017) can accumulate in their effluents as a source of point

pollution, which can be treated before they reach water bodies. The treatment of these effluents could be solved technologically with filtering materials where low cost is usually one of the main limiting factors.

In this study, montmorillonite-carbon nanocomposites (M-HC) were produced by hydrothermal carbonization of carbohydrates in presence of M sample. In a previous work, authors reported that similar M-HC materials showed higher reutilization capacity than that of M for norfloxacin (NOR) sorption (Zelaya Soulé et al., 2019). This behavior indicated that a deeper research on the synthesis conditions will be needed in order to improve the adsorption capacity of M-HC materials. Besides, the possible posterior microbiological treatment of the resultant M-HC-NOR materials could be favored in comparison to raw M samples (Yue et al., 2019). The M-HC hybrids synthesis on the present work was performed at various temperatures, times and using different types and concentrations of carbohydrates, as well as adding phosphoric acid at two concentrations as activating agent. SEM, porous texture characterization, XRD and FTIR analysis and zeta potential measurements, were used to characterize selected products and to evaluate structural and electrical surface charge changes produced by the synthesis conditions. Some materials were also chosen to study the chlorpyrifos (CPF) and thiabendazole (TBZ) adsorption capacity, and coagulation was also evaluated in order to assess their potential use as filters or reactors.

2. Materials and Methods

2.1 Materials

Na-montmorillonite (84%) labelled as M, was provided by Castiglioni Pes and Cia. (Lago Pellegrini deposit, Rio Negro, North Patagonia, Argentina) and used as received. The structural formula obtained from the chemical analysis was $[(Si_{3.89}Al_{0.11})(Al_{1.43}Fe^{3+}_{0.28}Mg_{0.30})O_{10}(OH)_2]Na^{+}_{0.41}$ and its main properties were: isoelectric point (IEP) pH = 2.7, total specific surface area (TSSA) = 621 $m^2 g^{-1}$, cationic exchange capacity (CEC) = 0.825 mmol g^{-1} (Gamba et al., 2015), and 31.4 cm^3 of swelling capacity (Magnoli et al., 2008)

Dextrose (D), cellulose (C) and cornstarch (AM) were used as carbon sources. All of them were analytical grade reagents, purchased from Anedra, MERCK, and Sigma Aldrich, respectively. C is a biopolymer of D. The H_3PO_4 (85%) was analytical grade from Chicarelli Lab., chosen as activating agent due to the low cost, the fact that is more environmental friendly than alkali hydroxide, by its possible industrial recovery after their use (Wang et al., 2011) and the better obtained material when it is used instead of H_2SO_4 (Mansouri et al., 2018).

Thiabendazole (TBZ) was from Fluka (Buchs, Switzerland) (98%). It´s IUPAC chemical formula is 2-(thiazol-4-yl) benzimidazole. Chlorpyrifos (CPF) was purchase at Clorfox Company (48%). All drugs were use as received without further purification.

The structure schema of both pesticides is shown in Fig. 1.

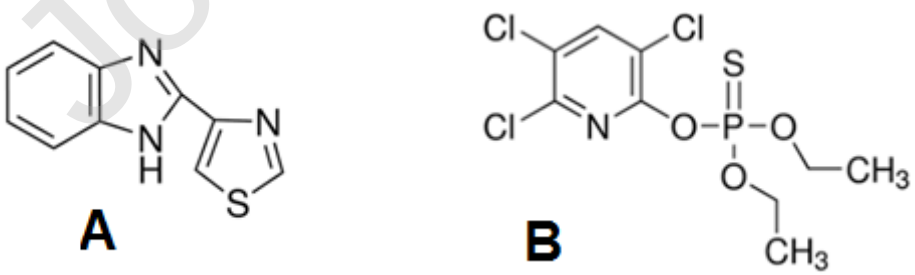

Fig. 1 Structure scheme of: A) Thiabendazole (TBZ) and B) Chlorpyrifos (CPF) pesticides.

2.2. Methods

2.2.1 Carbon synthesis by hydrothermal carbonization

In order to synthetize the M-HC hybrid, 50 mL of a suspension of 10 mg mL^{-1} of M sample in deionized water was sonicated for 3 h, and then a specific amount (to achieve a 5, 10 or 25 mg mL^{-1} concentration) of the selected carbohydrate (D, C or AM) was added. After, the suspension was heated (180 or 210 ºC) into a Teflon-lined autoclave during 16 or 24 h. The solid products were filtered and dried at 60 ºC overnight, ground and stored for further analysis. In some cases, acid activation was performed by the H_3PO_4 addition (0.17 or 0.33 % V/V, which were identified adding ac1 and ac2 labels, respectively) into the Teflon-lined autoclave before heat treatment. In order to evaluate the thermal and acid treatments effect on the carbohydrates and on M sample, same procedures indicated previously were performed on some carbohydrates (HC) without M sample and on M sample in absence of HC.

The products were labeled with the following code: M, indicating the clay presence, followed by the carbohydrate and concentration used, and the acid presence when corresponded (ac1 or ac2). Finally, the temperature and the time of the synthesis process were included. For example, the name MD10ac1-210-24 indicates that the synthesis was performed in presence of Montmorillonite with 10 mg mL^{-1} of Dextrose and phosphoric acid at 0.16% V/V at 210 °C for 24 h.

2.2.2. Samples characterization

The FE-SEM was performed on a Quanta FEG 650 microscope (FEI Company). Samples were fixed to 10mm metal mounts using carbon tape, and sputter coated with iridium under low pressure argon atmosphere.

Porous texture characterization was obtained from N_2 adsorption-desorption isotherms (>99.9995% pure) at -196 ºC and up to 1 atm measured in a volumetric apparatus ASAP-2010 (Micromeritics). Prior to the measurements, all samples were degassed overnight at 130 ºC under vacuum. The repeatability of the isotherms between different runs was better than 1.5%. The specific surface area was calculated applying the BET equation. Total pore volume (TPV) was calculated from the adsorbed amount at the relative pressure of 0.975.

X-ray diffraction (XRD) patterns were collected on powder samples using a Philips PW 1710 diffractometer operated at 40 kV and 35 mA with CuK_α radiation, in the range $3° < 2\theta < 70°$, with counting time of 2 s/step and step width of 0.040° (2θ).

Fourier transform infrared spectra (FTIR) were acquired using Nicolet 8700 Fourier Transformer Infrared Spectrometer with DTGS and MCT Detectors by averaging 64 scans in the 4000-400 cm^{-1} spectral range.

Electrokinetic potentials were determined using Brookhaven 90Plus/Bi-MAS with the electrophoretic mobility function. The electrophoretic mobility was converted into zeta potential values automatically using the Smoluchowski equation. For each determination, sample suspensions (1 g/L) were done on KCl 10^{-3} M solutions used as inert electrolyte and the pH value was adjusted to 4.5.

2.2.3. Adsorption experiments

A weighed amount of the respective pesticide was dissolved in deionized water in order to prepare a 25 mg L^{-1} solution. Additional concentrations were obtained by dilution the previous solution in deionized water. The adsorption experiments were carried out in batch conditions with a solid/ solution ratio of 8 g L^{-1}, a contact time of 24 h, at 20 ºC, under continuous stirring (150 rpm) and without pH adjustment. After the equilibration time, the suspensions were centrifuged at 14000 rpm for 15 min to separate the reaction products. The solid phases

resulting from the adsorption experiments were rinsed with distilled water, air dried, and stored for further analysis.

The concentration of TBZ in the supernatants was determined by a high performance liquid chromatograph (HPLC) coupled to UV–visible (λ = 298 nm) detector. The used column was a Shimadzu HPLC C18 (4.6 mm × 250 mm, 4.6 μm). The used mobile phase was a 70/30 methanol/water mixture flowing at 0.9 mL min^{-1}. The injected volume was 10 μL. The linear ranges of TBZ concentrations were within 0.5–25 mg/L (R^2 = 0.999).

The concentration of CPF in the supernatants was analyzed by HPLC equipment described above, at λ= 290 nm. The mobile phase was an 80/20 acetonitrile/water mixture flowing at 0.9 mL min^{-1}. The injected volume was 10 μL. The linear ranges of CPF concentrations were within 0.25–10 mg L^{-1} (R^2 = 0.999).

The adsorption percentage of TBZ or CPF was determined according to the following equations:

$$sorption\ (\%) = \frac{C_i - C_e}{C_i} * 100 \qquad eq\ (1)$$

where C_i and C_e represent the adsorbate concentration in solution before and after sorption experiments, respectively.

2.2.4. Coagulation experiments

The coagulation property was evaluated for M, Mac1-210-24, MD10-210-24 and MD25ac2-210-24 samples. To achieve this, 0.12 g of the indicated sample was suspended in 10 mL of water (Milli-Q), and photographs of the suspensions were taken after 0, 24 and 45 h of contact time.

3. Results and discussion

3.1 Characterization of the hydrothermal carbons

Fig. 2 revealed the different colors of the obtained products. Particularly, the light brown of raw M changed to orange and green color for M-210-24 and Mac1-210-24 samples, respectively. These color differences could be attributed to changes in the structural iron oxidation state (Eissa et al., 1994). The M-HC compounds showed dark brown (MC10ac1-180-16 sample) or black color (MD25-180-16 and MAMac1-210-24, samples) which revealed the M surface coating by carbonaceous materials (Zhang et al., 2015).

In particular, color of materials obtained at 180 °C from cellulose (C) was gray (Fig. 2 and Fig. S1 in supplementary material), which reveals an unfinished process of carbon formation, probably because this temperature is not enough to produce a complete hydrothermal carbonization of the cellulose biopolymer. On the contrary, samples synthesized from cellulose at 210 °C shown a dark color indicating that carbonization took place. Therefore, in the following syntheses a treatment temperature of 210 °C and 24 h were used for all materials tested to guarantee the complete carbon formation process.

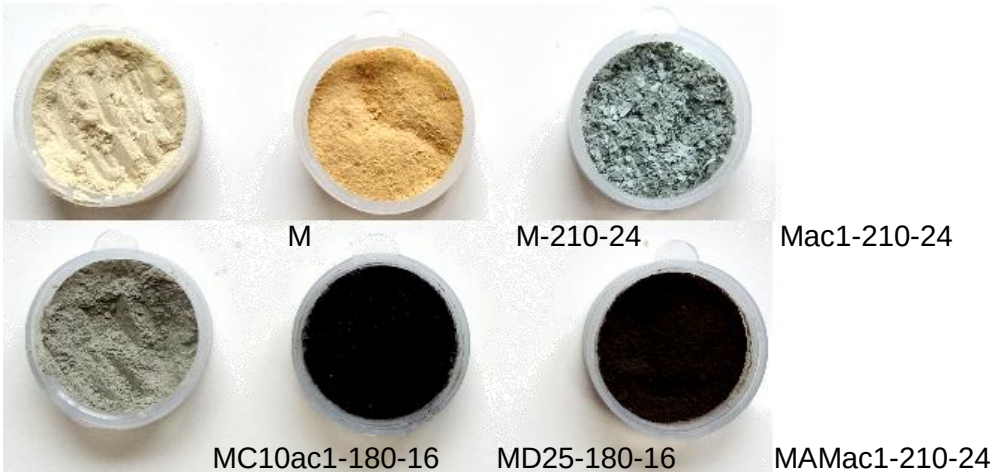

Fig. 2 Images of the obtained products.

SEM images of some representative samples were shown in Fig. 3. The SEM micrograph of M treated at 180 ºC, M-180-16 sample (Fig. 3a), showed a layered morphology characteristic of clays (Magaña et al., 2008). Composite materials prepared with carbohydrates showed, in general, the same-layered morphology but with greater roughness, probably due to the carbon layer deposited on the clay sheets (Fig. 3b). For samples prepared with carbohydrate concentration of 5 mg mL^{-1}, non-free carbon was observed (figure not shown). When the concentration used was 10 mg mL^{-1}, few carbon microspheres with size around 1 µm can be observed in some samples, e.g. Fig. 3c. The amount and size of these microspheres increase with the carbohydrate concentration used during the synthesis. Thus, carbon microspheres of around 2 µm (Fig. 3d) were observed for all samples prepared with the highest carbohydrate concentration studied here (25 mg mL^{-1}). These microspheres correspond to the expected morphology for hydrothermal carbon prepared by hydrothermal carbonization of carbohydrates (Titirici et al., 2008). Because our interest is to attain a material with the carbon integrates at the M surface, without isolated microspheres, the concentration of carbohydrates choose for the following synthesis was 10 mg mL^{-1}. In figures 3c and d also lower clay sheet than those of the M thermal treated sample (fig.3 a) can be identified, indicative of the M structure attack by the acid treatment (Hisarli, 2005).

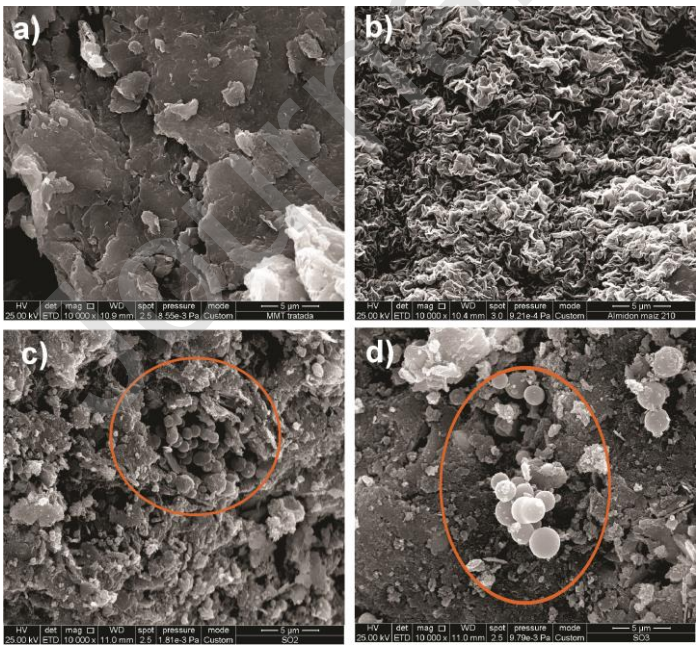

Fig. 3 SEM images of: a) M-180-16, b) MAM10-210-16, c) MD10ac2-210-16 and d) MD25ac2-210-16. The microspheres presence of free hydrochar was indicated within circles.

In order to evaluate changes in the specific surface and porosity of the studied samples, the BET surface area (Fig. 4) and total pore volume (Fig. 5) were determined. The M used in this work has a BET surface area of 66 $m^2 g^{-1}$. Hydrothermal treatments at 180 and 210 ºC cause the reduction of the BET surface area to 53 and 49 $m^2 g^{-1}$, respectively. This fact is attributed to the collapse of the interlayer space of M (as was corroborated by the absence of the reflection peak corresponding to d001 plane, and will be discussed in following paragraph), which produce a decrease of the available surface (Fernández et al., 2013; Torres Sánchez et al., 2011). Contrary, for an Australian bentonite an increases on specific surface area was observed when heating the samples at 100 ºC or 200 ºC in a muffle furnace (Toor and Jin, 2012). On the other hand, when the hydrothermal treatment at 210 ºC was carried out in the presence of phosphoric acid, an increase in the BET surface area was observed: Mac1 and Mac2 samples had 82 and 81 $m^2 g^{-1}$, respectively, as was also reported for an Australian sodium bentonite obtained by acid treatment (Toor and Jin, 2012). This increase in the surface area after activation of M with acids was assigned to the removal of metal-exchange cation (Mg^{2+}, Fe^{3+} and Al^{3+}) and proton exchange (Nguetnkam et al., 2005; Wang et al., 2010). In addition, for the Mac1 sample the structure was preserved despite the acid treatment, but not for the Mac2 sample where mainly the leaching of octahedral ions Al^{3+} modifies the M structure, as will be explained later.

The BET surface values of M-HC samples synthetized in the absence of acid were lower than that of M sample. The increase of the initial carbohydrate concentration (evaluated for dextrose, with 5, 10 and 25 mg mL^{-1}, at 180 °C and 16 h of treatment) did not evidence significant changes in the BET values (< 2.5 $m^2 g^{-1}$). This behavior was attributed to the pores obstruction by the HC formation (Zhang et al., 2015). The acid presence in the synthesis of M-HC materials produced higher surface area than those prepared by hydrothermal carbonization without phosphoric acid, increasing with the acid concentration used in the synthesis, and assigned to the partial decay of the lamellar structure of M sample (Wang et al., 2010). The evaluation of the carbohydrates initial content effect, contrarily to that evidenced for products without acid treatment, showed a significant decrease of the surface area (from 64.8 to 42.8 $m^2 g^{-1}$, for MD10ac2-210-16 and MD25ac2-210-16 samples, respectively). It is also worth noting that a time increase of thermal treatment (for 210 ºC) from 16 to 24 h, evaluated in the MHC25ac2 with dextrose as HC source, generated a decrease in the specific surface from 42.4 to 28.7 $m^2 g^{-1}$.

The thermal treatment of carbohydrates alone (irrespective of the carbohydrate used) generated products with very low surface values (Titirici and Antonietti, 2010), and the acid treatment seem does not influence this parameter (e.g. HC10-210-24 and HC10ac2-210-24 samples, in Fig. 4), being somewhat larger the surface values attained for HC coming from cellulose than for dextrose or cornstarch.

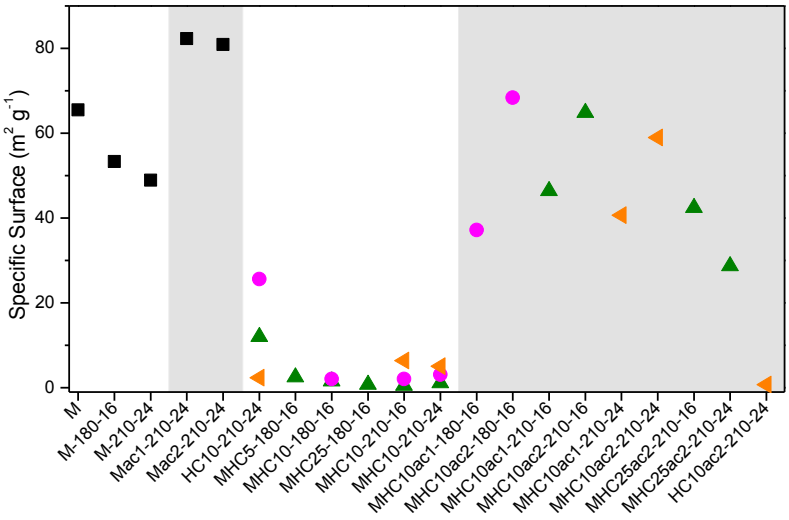

Fig. 4 Specific surface for the indicated samples. Grey zones highlight materials synthetized in acid presence. Symbols indicate: (■) M and M-HC samples with different carbohydrates (▲) dextrose, (●) cellulose, and (◀) cornstarch.

The Fig. 5 showed the total pore volume, TPV, values for the synthetized samples. The TPV of the montmorillonite decreases with the thermal treatment, as happened for surface area values, mainly originated by the drop of microporosity and collapse of the interlayer (Torres Sánchez et al., 2011). The increase of TPV values with the activation treatment (thermal treatment in the presence of phosphoric acid) could be assigned to the formation of porous silica product, as for the M acid activation with HCl (Temuujin et al., 2004). Unambiguously, the decrease found in the surface area values for M-HC samples, described in the previous section, can be assigned to the pores obstruction of M by HC originating the collapse of the TPV values of these samples (Fig. 5). Furthermore, an increase in the TPV values of all acid activated samples was observed, being higher for products prepared with the highest acid concentration. Thus, both series (M and M-HC samples) showed similar trends. Besides, the lower TPV value obtained for MHC25ac2 than MHC10ac2 samples (Fig. 5) was associated to a high obstruction of its pores due to a greater amount of HC deposited. For HC materials, the existence of small number of micropores (Titirici and Antonietti, 2010) regardless the initial carbohydrate and the used acid, produced the drop observed of TPV values in Fig. 5. In brief, it can be highlighted that the acid treatment recovers the loss of BET and TPV values of the M-HC samples, reaching those obtained for the raw M sample.

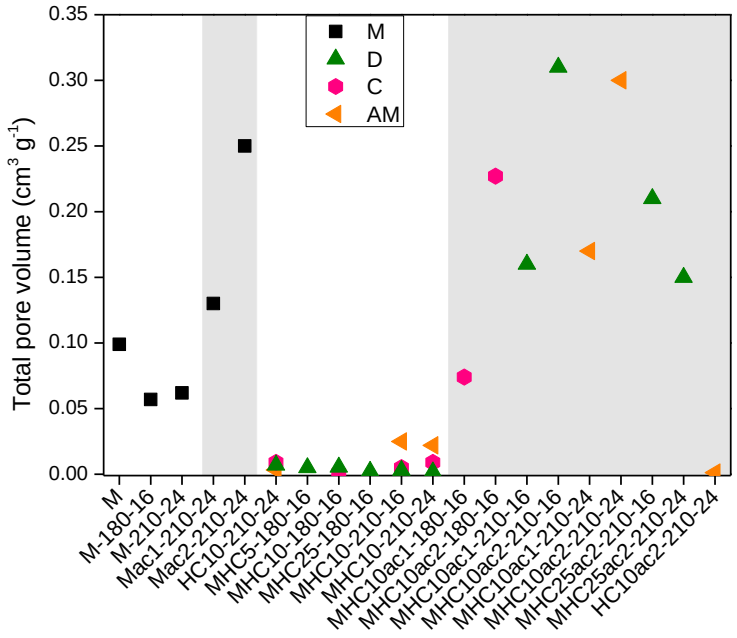

Fig. 5 Total pore volume of indicated samples. Grey zones highlight materials synthetized in acid presence. Symbols indicate: (■) M and M-HC samples with different carbohydrates (▲) dextrose, (●) cellulose, and (◀) cornstarch.

Total diffraction patterns of some samples (M, AM with thermal treatment, M with AM as HC source and thermal treatment, MAM10-210-24, and acid treatment, MAM10ac2-210-24 samples) were shown in Fig. 6, in order to evidence crystallinity changes among them. Typical X-ray diffractogram was found for M sample with d001 peaks at 6.9º and 6.18º (2θ) corresponding to 1.27 nm and 1.43 nm of the basal space and associated to the Na^{+} and Ca^{2+} presence in the interlayer space, respectively. The HC samples, represented by AM10-210-24 sample in Fig. 6, shown an amorphous large peak between 15º to 35º (2θ), which did not overlap the 001 peaks of M, and allowed to follow its shift by changes produced due to the different treatments at the M sample interlayer.

The XRD pattern of M sample and its thermal treated products up to 550 ºC was analyzed in previous work, and a decrease of the interlayer space of 0.03 nm resulted as the main structure modification (Torres Sánchez et al., 2011). The structural modification of M sample by phosphoric acid treatment, generate leaching of Al^{3+} ions from the octahedral sheet bringing a decrease in the intensity of 001 and 100 reflection peaks at 6.9º and 19.7 º(2θ) (or 1.27 and 0.45 nm, respectively). Particularly, the 001 peak shift to lower values indicating the relaxation of the structure in the *c* direction. In the Mac2-210-24 sample (Fig. S2 in supplementary material) peaks at 20.3; 21.4 y 23.0 º(2θ) (or 0.44, 0.41 and 0.37 nm, respectively) were assigned to tridymite phase (Freiding et al., 2007; Tanaka and Chikazawa, 1999; Xu et al., 1989), which remained in MAM10ac1-210-24 and MAM10ac2-210-24 samples (Fig. 6). Also, the quartz peak at 26.5 º(2θ) (0.34 nm) can be noticed in the acid treated M samples (Fig. 6) by the formation of amorphous silica (Trabelsi and Tlili, 2017)

The structural characteristic of M sample, as was indicated previously, remained in the M-HC products after thermal (MAM10-210-24 sample) or ac1 treatment (MAM10ac1-210-24), and similar results were obtained for all M-CH thermal and acid activated products (figures not shown). Particularly, the decrease of 060 reflection peak (62.0 º(2θ)) with increase of acid concentration treatment showed the decay of crystal structure (Torres Sánchez, 1997).

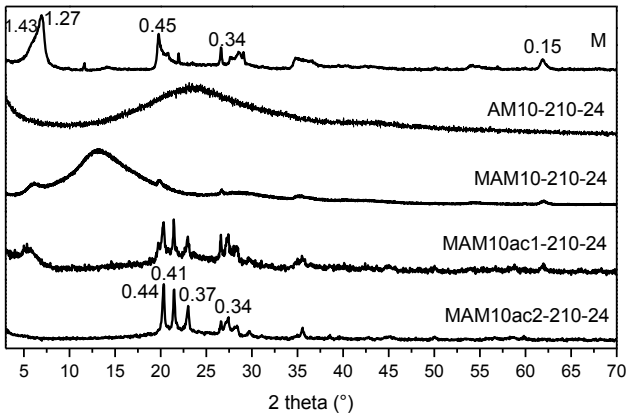

Fig. 6 XRD diffraction patterns of indicated samples. Basal space was indicated in nm

The effect of thermal treatment and HC loading in the M interlayer space, as was indicated previously, can be followed by the shift of the 001 reflection (Fig. 7). The shift of 001 for M sample with thermal and acid treatment was analyzed in previous paragraph.

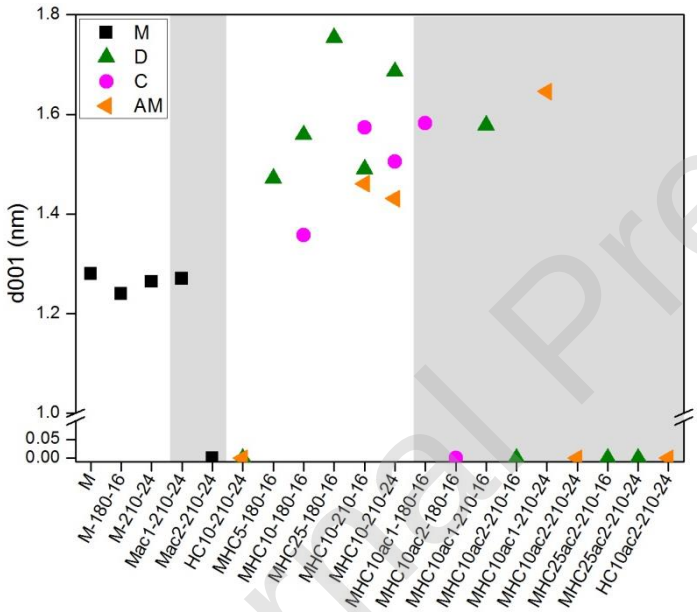

Fig. 7 Values of d001 of indicated samples. Grey zones highlight materials synthetized in acid presence. Symbols indicate: (■) M and M-HC samples with different carbohydrates (▲) dextrose, (●) cellulose, and (◀) cornstarch.

An increase of M basal space was observed in all M-HC products respect to that of M sample, indicating the HC incorporation in the M interlayer space, in agreement with previous findings (Li et al., 2014; Peng and Yang, 2017; Zhang et al., 2015). The increase of carbohydrate initial amount (showed in Fig. 7 for dextrose), generated an interlayer increase of 0.32, 0.45 and 0.51 nm, respect to that of M sample, for MD5-180-16, MD10-180-16 and MD25-180-16 samples, respectively. Comparison of different carbohydrates used (dextrose in MD10-180-16 and cellulose in MC10-180-16 samples), indicated a higher basal space increment for the M-HC sample with dextrose than that obtained with cellulose. This behavior could be assigned to the lower molecular size of D

respect to C carbohydrates, which could facilitate its incorporation to the M interlayer space (See Fig S3 in supplementary material), previous to the hydrothermal treatment. The temperature increase from 180 to 210 °C, with 16 h treatment, produced different interlayer values. An increase of 0.22 nm was found for MC10-180-16 respect to MC10-210-16 sample, while a decrease of around 0.26 nm appeared for MD10-180-16 respect to MD10-210-16 samples. This behavior could be assigned to the different carbon formation process within cellulose and dextrose at both temperatures, as indicated the color changes (Fig. 2, and Fig.S1 in supplementary materials). Regarding the used time in the HC synthesis, a 001 increase of 0.20 nm was only observed for MD10-210 sample when thermal treatment time was increased from 16 to 24 h, behavior that could be attributed to a higher carbon formation by this carbohydrate.

The use of lowest amount of acid studied here (ac1 samples) on M-HC caused an increase in d001 respect to same samples prepared without acid. This behavior was attributed previously to the relaxation of the structure of M sample (Trabelsi and Tlili, 2017). The further increase of acid concentration in all the M-HCac2 samples, as was indicated in Fig. 6 for MAM10ac2-210-24 sample, showed structure decay with disappearance of 001 reflection peak and increase of tridymite peaks.

The XRD results evidence the HC loading at the M interlayer space, which remained after low acid treatment, while high acid treatment produced a structure loss of the products obtained.

The Fig. 8 shows the infrared spectra of M, Mac1-210-24, MC10-210-24, C10-210-24, MC10-180-16, MC10ac1-180-16 and MC10ac2-180-16 samples as example of the different used treatments. Spectra of M sample shows typical montmorillonite bands (Amarasinghe et al., 2009; Madejová et al., 2002; Nascimento et al., 2015; Vicente-Rodríguez et al., 1996). Thus, a wide band between 3500-3300 (centered at 3436 cm^{-1}) can be assigned to O-H stretching, with intramolecular hydrogen bridges of adsorbed water. The band at 1640 cm^{-1} also corresponds to adsorbed water molecules (O-H bending). Bands corresponding to stretching (3633 cm^{-1}) and deformation (932 cm^{-1}) vibrations of Al-OH-Al and Al-OH deformation vibration (1111 cm^{-1}) and Si–O stretching vibration at 1251 cm^{-1} are observed. Finally, a small peak at 1841 cm^{-1}, and present in all spectra, can be assigned to O-H bending vibration band in H-feldspar (Behrens and Müller, 1995), which is an impurity (12%) of the montmorillonite used in this work (Magnoli et al., 2008).

The Mac1-210-24 sample has the same FTIR spectra that M sample (Fig. 8a), with only a decrease in the relative intensity of Al-OH-Al vibration bands (3633 and 932 cm^{-1}), which indicates that the acidic treatment preferentially attacks the octahedral layers (Bieseki et al., 2013; Özcan and Özcan, 2004).

Hydrothermal carbon obtained from cellulose treated at 210 ºC for 24h (C10-210-24) has typical FTIR spectra of a polysaccharide hydrothermally carbonized (Fig. 8a), showing bands of aliphatic and aromatic hydrocarbons, and several O-containing functional groups (Yu et al., 2012). Thus, FTIR spectra of C10-210-24 sample showed the following bands: hydroxyls (O-H stretching (3500-3300 cm^{-1}), C-O stretching of alcohols (1023 cm^{-1}); C-H asymmetrical and symmetrical stretching (2960, 2928 and 2871 cm^{-1}) and C-H bending (1453 and 1400 cm^{-1}) in aliphatic and aromatic compounds; C=O stretching of carboxylic acids (1701 cm^{-1}) and C-O stretching (1308, 1234 cm^{-1}) in aromatic ethers and phenols and C=C aromatic skeletal stretching (1610 cm^{-1}). Hydrothermal carbons obtained from the other precursor shown similar FTIR spectra (Park and Kim, 2005).

Hybrid materials (M-HC) prepared by hydrothermal carbonization of saccharides in presence of montmorillonite have FTIR spectra that could be considered a mixture of HTC and M spectra, see for example FTIR spectra of MC10-210-24 sample in Fig. 8a. Additionally to bands from M and C10-201-24, three new peaks between 2200 and 2000 cm^{-1} were observed, which can be assigned to Si-H stretching vibrations in silanes

(Socrates, 2001), indicating the formation of chemical bonds between the clay and the saccharide during the hydrothermal carbonization.

FTIR spectra of the hybrids materials prepared using cellulose as precursor and carbonized at 180 ºC for 16h, both with or without adding phosphoric acid are represented in Fig. 8b. The hydrothermal carbonization temperature used has an effect on the FTIR spectra, producing a greater degree of carbonization and aromatization for sample prepared at the highest temperature. Thus, a higher intensity of the characteristic bands of the pyranose ring (C-O-C) at 1160 cm^{-1} and others bands in the same region, which correspond to C-O vibrations are observed for samples carbonized at 160 °C comparing to those prepared at 210 °C. Besides, the amount of acid has lower effect than the temperature, although in the same way (favoring the carbonization of carbohydrates) as it is reflected in a slight decrease in the relative intensity of the bands in the region between 1200-1000 cm^{-1}, for samples prepared in the presence of phosphoric acid.

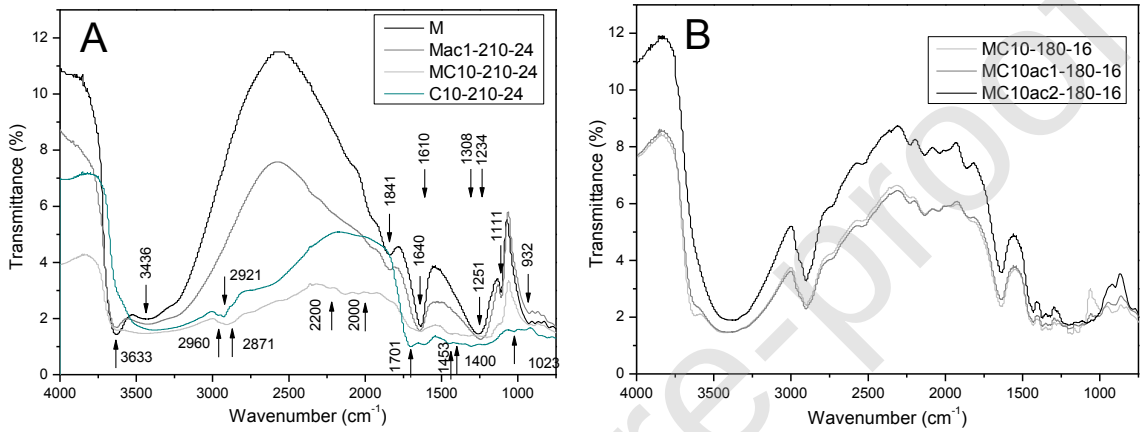

Fig. 8 Infrared spectra of: a) M, Mac1-210-24, MC10-210-24 and C10-210-24; b) MC10-180-16, MC10ac1-180-16 and MC10ac2-180-16 samples.

Zeta potential values of some samples at pH 4.5 were shown in Fig. 9. The negative zeta potential (around -28 mV) observed for Mt sample is assigned to the predominance of the negative charges on the particle faces with respect to the positive charge coming from the edges (Fernández et al. 2013). The increase of negative zeta potential value produced by the thermal treatment of M sample (to -35 and -30 mV for M-180-16 and M-210-24 samples, respectively) in agreement with results of our previous work (Fernández et al., 2013). The further acid treatment of thermal M samples produced a subsequent decrease of negative zeta potential values attaining values of around -23 mV (for Mac1-210-24 and Mac2-210-24 samples) consigned to a deep depopulation of the clay octahedral layer generated by the acid treatment (Breen et al., 1995), and consequently a free aluminium coating of the M surface (Torres Sánchez, 1997).

The HC10-210-24 samples, coming from cornstarch and cellulose as starting carbohydrates (Fig. 9), presented zeta potential values around -34 mV, while for sample coming from dextrose attained only -25 mV (Yu et al., 2012). Particularly, the acid treatment applied at cornstarch carbohydrate (HC10ac2-210-24 sample) decreased its initial negative zeta potential value from -35 to -19 mV, due to formation of carboxylic acid as indicated the FTIR analysis.

The initial amount of dextrose increase in M samples from 5 to 10 mg mL^{-1} at 180 °C and 16 h (for MHC5-180-16 and MHC10-180-16 samples, respectively), generated an increase of the negative zeta potential value

from -20 to -28 mV. The close zeta potential value of the MHC10-180-16 sample to that of dextrose hydrothermal product would indicate a higher presence of that product at the external surface. The similar zeta potential value, within the error method, obtained for further dextrose addition (MHC25-180-16 sample) could indicate the full coverage of external surface by the dextrose hydrothermal product. To understand more clearly the changes found in zeta potential values of these samples, further investigations are still needed, which are now in progress.

The temperature increases from 180 to 210 ºC for 16 h time treatment, in M-HC compounds (see zeta potential value of MD10-180-16 and MD10-210-16 samples, in Fig. 9) produced no changes of negative zeta potential value, within the method error. Moreover, the increase of thermal treatment time (see zeta potential value of MD10-210-16 and MD10-210-24 samples, in Fig. 9), produced 4 mV decrease of the negative zeta potential values, that can be assigned to the effect of temperature increase of the thermal treatment on M sample (as mentioned above).

The acid concentration increase for M-HC compounds, and thermal treatment for 16 h or 24 h with 10 mg ml^{-1} cellulose or cornstarch, respectively as HC sources, produced a decrease of negative zeta potential values within these samples and respect to the respective initial M-HC compounds. This behavior could be assigned to the formation of carboxylic acid from these HC compounds, as was evaluated for cornstarch hydrocarbon. However, for M-HC compound obtained with 10 mg ml^{-1} dextrose as hydrocarbon source, the acid concentration increase generated a 3 mV increase of negative zeta potential value while acid treatment with initial 25 mg ml^{-1} dextrose produced a decrease of negative zeta potential value as that found for others HC sources.

Summing up the results found, it could be highlight that type of carbohydrate initially present and acid treatment performed were the main factors that modify the negative zeta potential values of the products obtained.

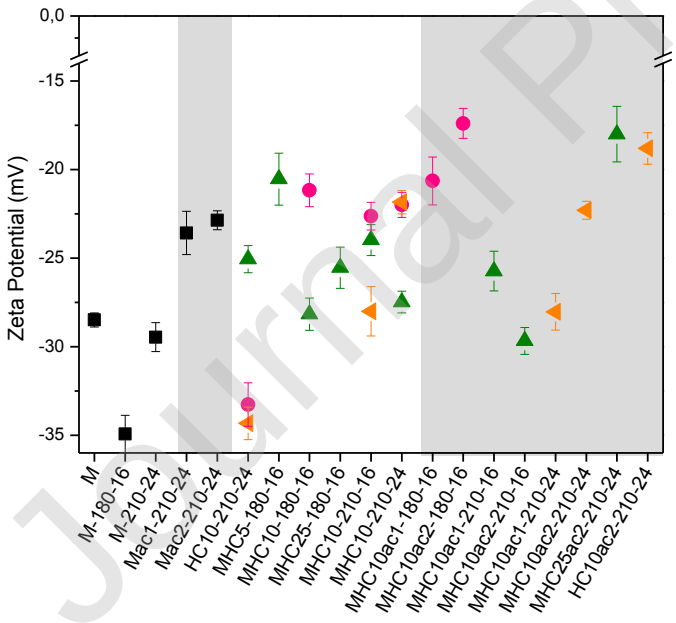

Fig. 9 Zeta potential values at pH 4.5 for indicated samples. Symbols indicate: (■) M and M-HC samples with different carbohydrates (▲) dextrose, (●) cellulose, and (◀) cornstarch.

3.2 Adsorption experiments

In Fig. 10 the adsorption percentage of TBZ and CPF in some representative samples can be found. Only a few samples were selected to this study because there were no large differences in the characterization results of

the different materials evaluated. The TBZ adsorption percentage obtained for M sample, agree with previous work (Lombardi et al., 2003), and was assigned to cationic exchange between interlayer Na^+, and/or adsorption on the external negative surface sites of M sample (Torres Sánchez et al., 2011) and the protonated TBZ. Whilst the CPF adsorption was assigned previously to physical interaction with the M surface, where the hydrolysis was inhibited (Wu and Laird, 2004).

The acid and thermal treatments performed on Mac1-210-24 sample produced similar percentage of TBZ and CPF adsorptions than those found for M sample. This could be attributed to the fact that the interlayer space (Fig. 7), and the electric surface charge (Fig. 9) were not affected by the treatments although the specific surface value increase more than 30% (Fig. 4). However, the important decrease of specific surface value for MD10 products (MD10-180-16 and MD10-210-24 samples), remaining the interlayer and negative electric surface charge, respect to M sample seems to be the responsible of the slight decrease on both pesticides percentage adsorption.

The acid treatment performed on MD10ac2-210-16 and MD25ac2-210-24 samples, which preserved the negative electric surface charge (Fig. 9), and where the collapse of the interlayer (Fig. 7) could be compensated by the increase of the specific surface area (Fig. 4), did not modify the TBZ adsorption percentages respect to that found for M sample. However, the structure modification indicated by the interlayer collapse, despite the increase of the specific surface area generated by the acid treatment decreased the CPF adsorption percentages of MD25ac2-210-24 sample respect to that of M sample.

The high adsorption percentages of both pesticides by the M-HC compounds evaluated encourage to attain the objective proposed, that is them use as filters or reactors.

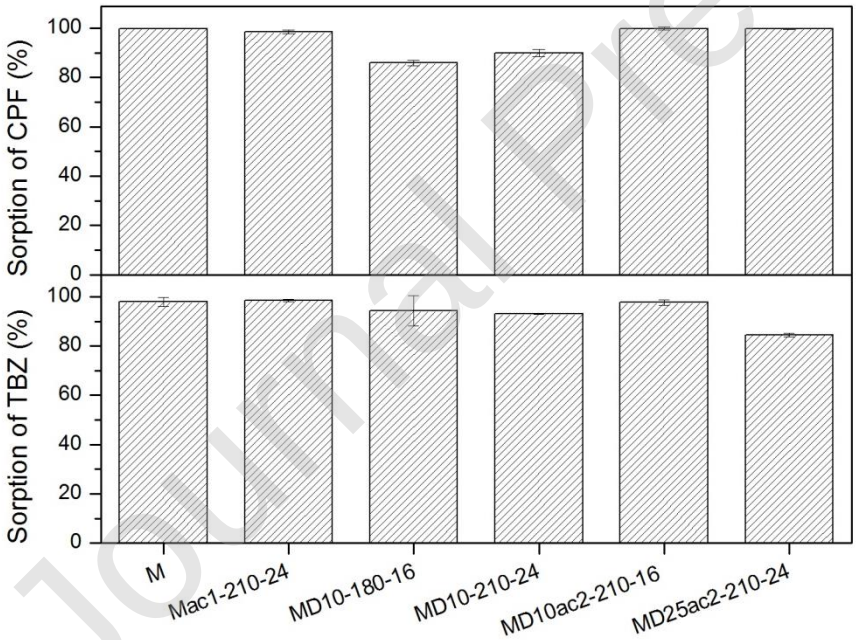

Fig. 10: Sorption percentages of CPF and TBZ at indicated samples**.**

3.2 Coagulation experiments

Fig. 11 showed coagulation results for M, Mac1-210-24, MD10-210-24 and MD25ac2-210-24 samples at 0, 24 and 45 h, respectively. The resulted clarity of the solution demonstrated the coagulation capacity of all studied samples. Both M-HC samples showed translucent solutions after 24 h. The MD25ac2-210-24 sample attained the best coagulation performance than the other samples evaluated. Besides, the acid activation

performed in Mac1-210-24 sample improved its coagulation performance respect to M sample. In technology process is important the use of a cheap material with great adsorbent capacity and simple manipulation. The results obtained it is work showed that the materials proposed present similar adsorption capacity and better coagulation performance than M sample. In addition, although these products are not cheaper than the raw M sample, the cost of synthesis is not high and does not constitute harm to the environment. Summing up results obtained encourage the application studies of the products evaluated.

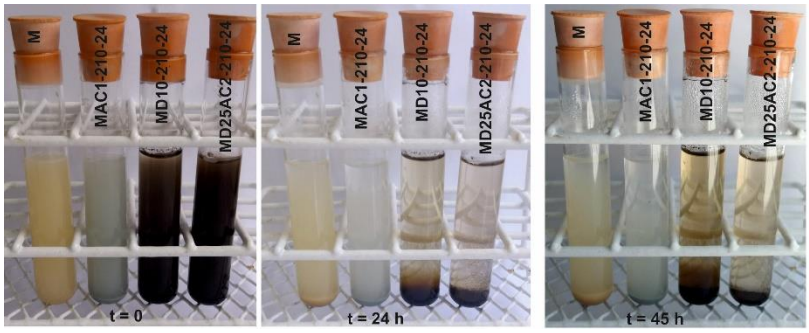

Fig. 11: Coagulation of indicated samples at t= 0, 24 and 45 h.

4. Conclusions

The synthesis of hydrothermal carbons in montmorillonite presence was carried out in order to evaluate the effect of different synthesis conditions (time, temperature, type and concentration of carbohydrates and acid treatment). The selected carbohydrate concentration was 10 mg mL^{-1} due to presence of carbon associated to the M surface and the absence of free carbon as indicated by SEM results. This behavior that was validated by the lower surface area values found for M-HC than for M sample, pointing out a coating effect of the M surface by the HC products. The acid activation process increased the specific surface area of the M-HC products, generated by the partial destruction of the M structure, as revealed the d001 and d060 reflection peaks disappearance, as a function of the acid concentration. Besides, as the incorporation to the M interlayer space of dextrose was facilitated, this carbohydrate was proposed as the best carbon source in order to have a better interaction between the HC and M sample. The M-HC samples presented FTIR bands corresponding to both M and HC samples, revealing the presence of HC in the surface of M sample, in agreement with that observed by SEM. Zeta potential measurements, at pH 4.5, for all samples showed similar negative values to that of M sample. This behavior is related to the conservation of the TBZ and CPF adsorption percentages, with respect to that of the sample M.

Taking into account the similar adsorption percentage values achieved by M-HC and M samples and the significant increase of the coagulation capacity of all M-HC compounds evaluated, these materials could be proposed to remove TBZ and CPF in filters or reactors. It would be necessary a further study related to determine the optimal adsorption conditions using MD10ac1-210-24 and MD10ac2-210-24 as adsorbent materials, where also the acid concentration used in the synthesis process would be evaluated.

Acknowledgments

Financial support of Argentine Ministry of Science, Technology and Innovation – PICT 2014/ 585 and Spanish Ministry of Economy and Competitiveness program Scientific cooperation for development i-Coop 2016 soils and legumes project 2016SU0006 are gratefully acknowledged. M.A.F., M.L.M and R.M.T.S. are

members of National Council of Scientific and Technological Research (CONICET) and M.E.Z.S. acknowledged CONICET fellowship.

References

Abbas, M., Adil, M., Ehtisham-ul-Haque, S., Munir, B., Yameen, M., Ghaffar, A., Shar, G.A., Asif Tahir, M., Iqbal, M., 2018. Vibrio fischeri bioluminescence inhibition assay for ecotoxicity assessment: A review. Sci. Total Environ. 626, 1295–1309. https://doi.org/10.1016/j.scitotenv.2018.01.066

Amarasinghe, P.M., Katti, K.S., Katti, D.R., 2009. Nature of organic fluid-montmorillonite interactions: An FTIR spectroscopic study. J. Colloid Interface Sci. 337, 97–105. https://doi.org/10.1016/j.jcis.2009.05.011

Basnayaka, L., Subasinghe, N., Albijanic, B., 2018. Influence of clays on fine particle filtration. Appl. Clay Sci. 156, 45–52. https://doi.org/10.1016/j.clay.2018.01.008

Behrens, H., Müller, G., 1995. An infrared spectroscopic study of hydrogen feldspar (HA1Si3O8). Mineral. Mag. 59, 15–24. https://doi.org/10.1180/minmag.1995.59.394.02

Bieseki, L., Bertell, F., Treichel, H., Penha, F.G., Pergher, S.B.C., 2013. Acid treatments of montmorillonite-rich clay for Fe removal using a factorial design method. Mater. Res. 16, 1122–1127. https://doi.org/10.1590/s1516-14392013005000114

Breen, C., Madejová, J., Komadel, P., 1995. Correlation of catalytic activity with infra-red, 29Si MAS NMR and acidity data for HCl-treated fine fractions of montmorillonites. Appl. Clay Sci. 10, 219–230. https://doi.org/10.1016/0169-1317(95)00024-X

Capra, A., Scicolone, B., 2004. Emitter and filter tests for wastewater reuse by drip irrigation. Agric. Water Manag. 68, 135–149. https://doi.org/10.1016/j.agwat.2004.03.005

Chham, A., Khouya, E.H., Oumam, M., Abourriche, A., Gmouh, S., Mansouri, S., Elhammoudi, N., Hanafi, N., Hannache, H., 2018. The use of insoluble mater of Moroccan oil shale for removal of dyes from aqueous solution. Chem. Int. 4, 67–76.

Chikwe, T.N., Ekpo, R.E., Okoye, I., 2018. Competitive adsorption of organic solvents using modified and unmodified calcium bentonite clay mineral. Chem. Int. 4, 230–239.

Eissa, N.A., Sheta, N.H., Meligy, W.M. El, Sallam, H.A., 1994. Mössbauer effect study of the effect of gamma irradiation and heat treatment on montmorillonite. Hyperfine Interact. 91, 783–787. https://doi.org/10.1007/BF02064607

Fernández, M., Alba, M.D., Torres Sánchez, R.M., 2013. Effects of thermal and mechanical treatments on montmorillonite homoionized with mono- and polyvalent cations: Insight into the surface and structural changes. Colloids Surfaces A Physicochem. Eng. Asp. 423, 1–10. https://doi.org/10.1016/j.colsurfa.2013.01.040

Freiding, J., Patcas, F.C., Kraushaar-Czarnetzki, B., 2007. Extrusion of zeolites: Properties of catalysts with a novel aluminium phosphate sintermatrix. Appl. Catal. A Gen. 328, 210–218. https://doi.org/10.1016/j.apcata.2007.06.017

Gamba, M., Flores, F.M., Madejová, J., Sánchez, R.M.T., 2015. Comparison of imazalil removal onto montmorillonite and nanomontmorillonite and adsorption surface sites involved: An approach for agricultural wastewater treatment. Ind. Eng. Chem. Res. 54, 1529–1538. https://doi.org/10.1021/ie5035804

Gamba, M., Kovář, P., Pospíšil, M., Torres Sánchez, R.M., 2017. Insight into thiabendazole interaction with montmorillonite and organically modified montmorillonites. Appl. Clay Sci. 137, 59–68.

https://doi.org/10.1016/j.clay.2016.12.001

Gao, N.F., Kume, S., Watari, K., 2005. Zeolite-carbon composites prepared from industrial wastes: (I) Effects of processing parameters. Mater. Sci. Eng. A 399, 216–221. https://doi.org/10.1016/j.msea.2005.04.008

Geise, G.M., Lee, H.S., Miller, D.J., Freeman, B.D., McGrath, J.E., Paul, D.R., 2010. Water purification by membranes: The role of polymer science. J. Polym. Sci. Part B Polym. Phys. 48, 1685–1718. https://doi.org/10.1002/polb.22037

Gottschall, N., Boutin, C., Crolla, A., Kinsley, C., Champagne, P., 2007. The role of plants in the removal of nutrients at a constructed wetland treating agricultural (dairy) wastewater, Ontario, Canada. Ecol. Eng. 29, 154–163. https://doi.org/10.1016/j.ecoleng.2006.06.004

Gu, Z., Gao, M., Lu, L., Liu, Y., Yang, S., 2015. Montmorillonite Functionalized with Zwitterionic Surfactant as a Highly Efficient Adsorbent for Herbicides. Ind. Eng. Chem. Res. 54, 4947–4955. https://doi.org/10.1021/acs.iecr.5b00438

Gun'ko, V.M., Skubiszewska-Zieba, J., Leboda, R., Turov, V. V., 2004. Impact of thermal and hydrothermal treatments on structural characteristics of silica gel Si-40 and carbon/silica gel adsorbents. Colloids Surfaces A Physicochem. Eng. Asp. 235, 101–111. https://doi.org/10.1016/j.colsurfa.2004.01.012

Guo, S., Dong, X., Wu, T., Zhu, C., 2016. Influence of reaction conditions and feedstock on hydrochar properties. Energy Convers. Manag. 123, 95–103. https://doi.org/10.1016/j.enconman.2016.06.029

Haynes, D., Müller, J., Carter, S., 2000. Pesticide and herbicide residues in sediments and seagrasses from the Great Barrier Reef World Heritage Area and Queensland Coast. Mar. Pollut. Bull. 41, 279–287. https://doi.org/10.1016/S0025-326X(00)00097-7

Hisarli, G., 2005. The effects of acid and alkali modification on the adsorption performance of fuller's earth for basic dye. J. Colloid Interface Sci. 281, 18–26. https://doi.org/10.1016/j.jcis.2004.08.089

Hunt, L., Bonetto, C., Resh, V.H., Buss, D.F., Fanelli, S., Marrochi, N., Lydy, M.J., 2016. Insecticide concentrations in stream sediments of soy production regions of South America. Sci. Total Environ. 547, 114–124. https://doi.org/10.1016/j.scitotenv.2015.12.140

Iqbal, M., 2016. Vicia faba bioassay for environmental toxicity monitoring: A review. Chemosphere 144, 785–802. https://doi.org/10.1016/j.chemosphere.2015.09.048

Jiménez, B., Chávez, A., Hernández, C., 1999. Alternative treatment for wastewater destined for agricultural use. Water Sci. Technol. 40, 355–362. https://doi.org/10.1016/S0273-1223(99)00518-1

Kausar, A., Iqbal, M., Javed, A., Aftab, K., Nazli, Z. i. H., Bhatti, H.N., Nouren, S., 2018. Dyes adsorption using clay and modified clay: A review. J. Mol. Liq. 256, 395–407. https://doi.org/10.1016/j.molliq.2018.02.034

Lagaly, G., Ogawa, M., Dékány, I., 2006. Chapter 7.3 Clay Mineral Organic Interactions. Dev. Clay Sci. https://doi.org/10.1016/S1572-4352(05)01010-X

Li, T., Shen, J., Huang, S., Li, N., Ye, M., 2014. Hydrothermal carbonization synthesis of a novel montmorillonite supported carbon nanosphere adsorbent for removal of Cr (VI) from waste water. Appl. Clay Sci. 93–94, 48–55. https://doi.org/10.1016/j.clay.2014.02.015

Liu, S., Sun, J., Huang, Z., 2010. Carbon spheres/activated carbon composite materials with high Cr(VI) adsorption capacity prepared by a hydrothermal method. J. Hazard. Mater. 173, 377–383. https://doi.org/10.1016/j.jhazmat.2009.08.086

Lombardi, B., Baschini, M., Torres Sánchez, R.M., 2003. Optimization of parameters and adsorption mechanism of thiabendazole fungicide by a montmorillonite of North Patagonia, Argentina. Appl. Clay Sci. 24, 43–50. https://doi.org/10.1016/j.clay.2003.07.005

Madejová, J., Janek, M., Komadel, P., Herbert, H.-J., Moog, H.C., 2002. FTIR analyses of water in MX-80 bentonite compacted from high salinary salt solution systems. Appl. Clay Sci. 20, 255–271. https://doi.org/https://doi.org/10.1016/S0169-1317(01)00067-9

Magaña, S.M., Quintana, P., Aguilar, D.H., Toledo, J.A., Ángeles-Chávez, C., Cortés, M.A., León, L., Freile-Pelegrín, Y., López, T., Sánchez, R.M.T., 2008. Antibacterial activity of montmorillonites modified with silver. J. Mol. Catal. A Chem. 281, 192–199. https://doi.org/10.1016/j.molcata.2007.10.024

Magnoli, A.P., Tallone, L., Rosa, C.A.R., Dalcero, A.M., Chiacchiera, S.M., Torres Sanchez, R.M., 2008. Commercial bentonites as detoxifier of broiler feed contaminated with aflatoxin. Appl. Clay Sci. 40, 63–71. https://doi.org/10.1016/j.clay.2007.07.007

Mansouri, S., Elhammoudi, N., Mouiya, M., Makouki, L., Chham, A., 2018. Elaboration of novel adsorbent from Moroccan oil shale using Plackett – Burman design. Chem. Int. 4, 7–14.

Marino, D., Ronco, A., 2005. Cypermethrin and chlorpyrifos concentration levels in surface water bodies of the Pampa Ondulada, Argentina. Bull. Environ. Contam. Toxicol. 75, 820–826. https://doi.org/10.1007/s00128-005-0824-7

Martín-Jimeno, F.J., Suárez-García, F., Paredes, J.I., Martínez-Alonso, A., Tascón, J.M.D., 2015. Activated carbon xerogels with a cellular morphology derived from hydrothermally carbonized glucose-graphene oxide hybrids and their performance towards CO2 and dye adsorption. Carbon . 81, 137–147. https://doi.org/10.1016/j.carbon.2014.09.042

Nascimento, A.R. do, Alves, J.A.B.L.R., Melo, M.A. de F., Melo, D.M. de A., Souza, M.J.B. de, Pedrosa, A.M.G., 2015. Effect of the Acid Treatment of Montmorillonite Clay in the Oleic Acid Esterification Reaction. Mater. Res. 18, 283–287. https://doi.org/10.1590/1516-1439.293014

Nguetnkam, J.P., Kamga, R., Villiéras, F., Ekodeck, G.E., Razafitianamaharavo, A., Yvon, J., 2005. Assessment of the surface areas of silica and clay in acid-leached clay materials using concepts of adsorption on heterogeneous surfaces. J. Colloid Interface Sci. 289, 104–115. https://doi.org/10.1016/j.jcis.2005.03.053

Nir, S., Undabeytia, T., Yaron-Marcovich, D., El-Nahhal, Y., Polubesova, T., Serban, C., Rytwo, G., Lagaly, G., Rubin, B., 2000. Optimization of adsorption of hydrophobic herbicides on montmorillonite preadsorbed by monovalent organic cations: Interaction between phenyl rings. Environ. Sci. Technol. 34, 1269–1274. https://doi.org/10.1021/es9903781

Özcan, A.S., Özcan, A., 2004. Adsorption of acid dyes from aqueous solutions onto acid-activated bentonite. J. Colloid Interface Sci. 276, 39–46. https://doi.org/10.1016/j.jcis.2004.03.043

Park, S.J., Kim, B.J., 2005. Roles of acidic functional groups of carbon fiber surfaces in enhancing interfacial adhesion behavior. Mater. Sci. Eng. A. https://doi.org/10.1016/j.msea.2005.08.129

Peng, K., Yang, H., 2017. Carbon hybridized montmorillonite nanosheets: preparation, structural evolution and enhanced adsorption performance. Chem. Commun. 53, 6085–6088. https://doi.org/10.1039/C7CC02334K

Regaldo, L., Gutierrez, M.F., Reno, U., Fernández, V., Gervasio, S., Repetti, M.R., Gagneten, A.M., 2018. Water and sediment quality assessment in the Colastiné-Corralito stream system (Santa Fe, Argentina): impact of industry and agriculture on aquatic ecosystems. Environ. Sci. Pollut. Res. 25, 6951–6968. https://doi.org/10.1007/s11356-017-0911-4

Santiago, C.C., Fernández, M.A., Torres Sánchez, R.M., 2016. Adsorption and characterization of MCPA on DDTMA- and raw-montmorillonite: Surface sites involved. J. Environ. Sci. Heal. - Part B Pestic. Food Contam. Agric. Wastes 51, 245–253. https://doi.org/10.1080/03601234.2015.1120618

Schipper, P.N.M., Vissers, M.J.M., van der Linden, A.M.A., 2008. Pesticides in groundwater and drinking water wells: Overview of the situation in the Netherlands. Water Sci. Technol. 57, 1277–1286. https://doi.org/10.2166/wst.2008.255

Socrates, G., 2001. Infrared and Raman characteristic group frequencies, third edition, John Wiley & Sons, LTD. https://doi.org/10.1002/jrs.1238

Tanaka, H., Chikazawa, M., 1999. Formation and structure of titanium alkyl phosphates. R. Soc. Chem. 254, 331–337. https://doi.org/10.1006/jcis.2002.8622

Temuujin, J., Jadambaa, T., Burmaa, G., Erdenechimeg, S., Amarsanaa, J., MacKenzie, K.J.D., 2004. Characterisation of acid activated montmorillonite clay from Tuulant (Mongolia). Ceram. Int. 30, 251–255. https://doi.org/10.1016/S0272-8842(03)00096-8

Titirici, M.M., Antonietti, M., 2010. Chemistry and materials options of sustainable carbon materials made by hydrothermal carbonization. Chem. Soc. Rev. 39, 103–116. https://doi.org/10.1039/b819318p

Titirici, M.M., Antonietti, M., Baccile, N., 2008. Hydrothermal carbon from biomass: A comparison of the local structure from poly- to monosaccharides and pentoses/hexoses. Green Chem. 10, 1204–1212. https://doi.org/10.1039/b807009a

Toor, M., Jin, B., 2012. Adsorption characteristics, isotherm, kinetics, and diffusion of modified natural bentonite for removing diazo dye. Chem. Eng. J. 187, 79–88. https://doi.org/10.1016/j.cej.2012.01.089

Torres Sánchez, R.M., 1997. Mechanochemical effects on physicochemical parameters of homoionic smectite. Colloids Surfaces A Physicochem. Eng. Asp. 127, 135–140. https://doi.org/10.1016/S0927-7757(97)00105-2

Torres Sánchez, R.M., Genet, M.J., Gaigneaux, E.M., dos Santos Afonso, M., Yunes, S., 2011. Benzimidazole adsorption on the external and interlayer surfaces of raw and treated montmorillonite. Appl. Clay Sci. 53, 366–373. https://doi.org/10.1016/j.clay.2010.06.026

Trabelsi, W., Tlili, A., 2017. Phosphoric acid purification through different raw and activated clay materials (Southern Tunisia). J. African Earth Sci. 129, 647–658. https://doi.org/10.1016/j.jafrearsci.2017.02.008

Vicente-Rodríguez, M.A., Bañares-Muñoz, M.A., Suarez, M., Lopez-Gonzalez, J.D.D., 1996. Comparative FT-IR study of the removal of octahedral cations and structural modifications during acid treatment of several silicates. Spectrochim. Acta - Part A Mol. Spectrosc. 52, 1685–1694. https://doi.org/10.1016/S0584-8539(96)01771-0

Wang, L., Guo, Y., Zou, B., Rong, C., Ma, X., Qu, Y., Li, Y., Wang, Z., 2011. High surface area porous carbons prepared from hydrochars by phosphoric acid activation. Bioresour. Technol. 102, 1947–1950. https://doi.org/10.1016/j.biortech.2010.08.100

Wang, T.H., Liu, T.Y., Wu, Di.C., Li, M.H., Chen, J.R., Teng, S.P., 2010. Performance of phosphoric acid activated montmorillonite as buffer materials for radioactive waste repository. J. Hazard. Mater. 173, 335–342. https://doi.org/10.1016/j.jhazmat.2009.08.091

Wu, J., Laird, D. a, 2004. Interactions of Chlorpyrifos with Colloidal Materials in Aqueous Systems. J. Environ. Qual. 33, 1765. https://doi.org/10.2134/jeq2004.1765

Xu, Y., Maddox, P.J., Thomas, J.M., 1989. Preparation and characterization of molecular sieves based on aluminium phosphate. Polyhedron 8, 819–826. https://doi.org/10.1016/S0277-5387(00)83852-8

Yu, L., Falco, C., Weber, J., White, R.J., Howe, J.Y., Titirici, M.M., 2012. Carbohydrate-derived hydrothermal carbons: A thorough characterization study. Langmuir 28, 12373–12383. https://doi.org/10.1021/la3024277

Yue, Y., Shen, C., Ge, Y., 2019. Biochar accelerates the removal of tetracyclines and their intermediates by altering soil properties. J. Hazard. Mater. 380, 120821. https://doi.org/10.1016/j.jhazmat.2019.120821

Zelaya Soulé, M.E., Barraqué, F., Flores, F.M., Torres Sánchez, R.M., Fernández, M.A., 2019. Carbon/montmorillonite hybrids with different activation methods: adsorption of norfloxacin. Adsorption 25, 1361–1373. https://doi.org/10.1007/s10450-019-00098-2

Zhang, R., Chen, C., Li, J., Wang, X., 2015. Preparation of montmorillonite@carbon composite and its application for U(VI) removal from aqueous solution. Appl. Surf. Sci. 349, 129–137. https://doi.org/10.1016/j.apsusc.2015.04.222

Zheng, Q., Morimoto, M., Takanohashi, T., 2017. Finding of coal organic microspheres during hydrothermal treatment of brown coal. Fuel 195, 143–150. https://doi.org/10.1016/j.fuel.2017.01.066

Supplementary Information

Montmorillonite- hydrothermal carbon nanocomposites: synthesis, characterization and evaluation of pesticides retention for potential treatment of agricultural wastewater

M.E. Zelaya Soulé[a], M.A. Fernández[a], M.L. Montes[b], F. Suárez-García[c], R.M. Torres Sánchez[a] and J.M. D. Tascón[c]

[a]*Centro de Tecnología de Recursos Minerales y Cerámica. CETMIC, CIC-CONICET CCT-La Plata, Camino Centenario y 506- M.B. Gonnet, Argentina.*
[b]*IFLP, CONICET CCT-La Plata, UNLP, La Plata, Argentina.*
[c]*Instituto Nacional del Carbón, INCAR-CSIC, Francisco Pintado Fe, 26, 33011, Oviedo, España.*

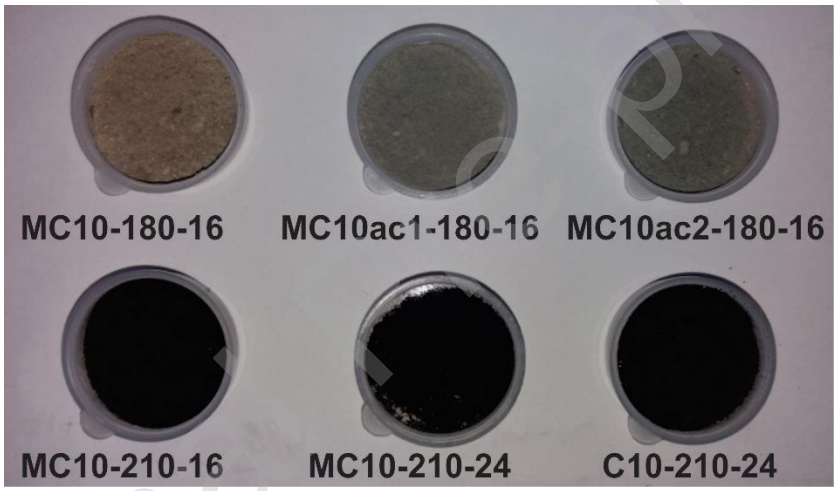

Fig. S1: Colors of the indicated products

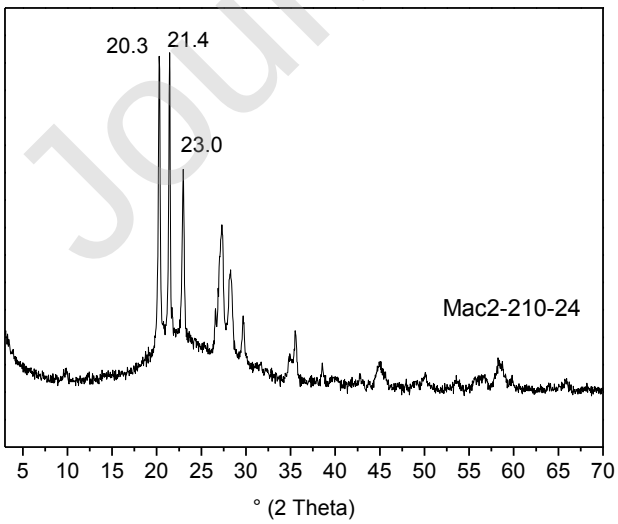

Fig. S2: DRX of Mac2-210-24.

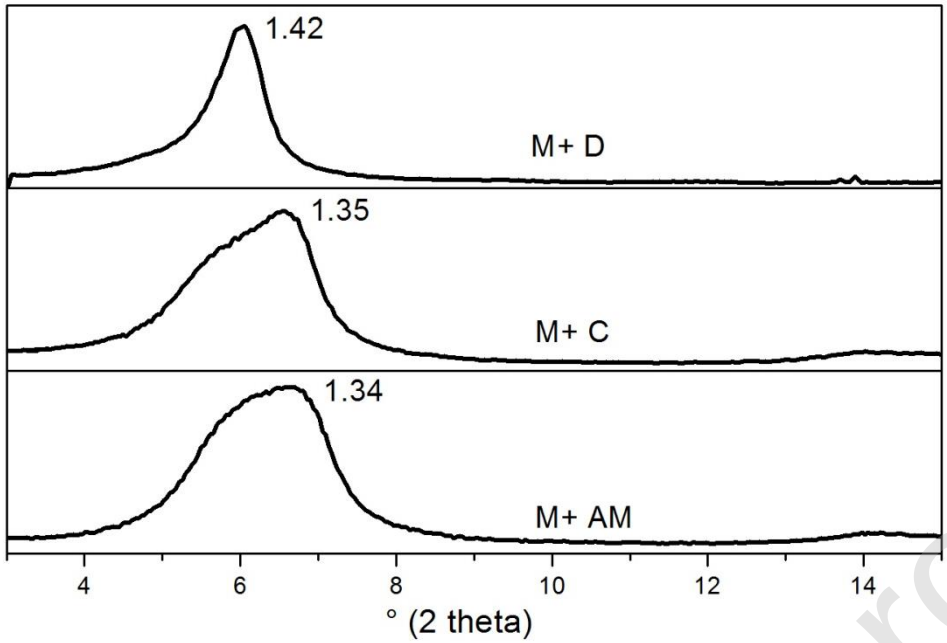

Fig. S3: DRX of mixtures of M sonicated during 3 h and indicated carbohydrates (at 10 mg mL^{-1})